# Spectral evidence for unidirectional charge density wave in detwinned BaNi2As2

Yucheng Guo,[1,2] Mason Klemm,[1] Ji Seop Oh,[1,3] Yaofeng Xie,[1] Bing-Hua Lei,[4] Luca Moreschini,[3,5] Cheng Chen,[6] Ziqin Yue,[1,7] Sergey Gorovikov,[8] Tor Pedersen,[8] Matteo Michiardi,[9,10,11] Sergey Zhdanovich,[9,10] Andrea Damascelli,[9,10] Jonathan Denlinger,[2] Makoto Hashimoto,[12] Donghui Lu,[12] Chris Jozwiak,[2] Aaron Bostwick,[2] Eli Rotenberg,[2] Sung-Kwan Mo,[2] Rob G. Moore,[13] Junichiro Kono,[1,14,15,16] Robert J. Birgeneau,[3] David J. Singh,[4,17] Pengcheng Dai,[1] and Ming Yi[1,*]

[1]*Department of Physics and Astronomy, Rice University, Houston, Texas 77005, USA*
[2]*Advanced Light Source, Lawrence Berkeley National Laboratory, Berkeley, California 94720, USA*
[3]*Department of Physics, University of California, Berkeley, California 94720, USA*
[4]*Department of Physics and Astronomy, University of Missouri, Columbia, Missouri 65211, USA*
[5]*Materials Science Division, Lawrence Berkeley National Laboratory, Berkeley, California 94720, USA*
[6]*Department of Physics, University of Oxford, Oxford OX1 3PU, United Kingdom*
[7]*Applied Physics Graduate Program, Smalley-Curl Institute, Rice University, Houston, Texas 77005, USA*
[8]*Canadian Light Source, Inc., 44 Innovation Boulevard, Saskatoon, SK S7N 2V3, Canada*
[9]*Department of Physics and Astronomy, University of British Columbia, Vancouver, British Columbia V6T 1Z1, Canada*
[10]*Quantum Matter Institute, University of British Columbia, Vancouver, British Columbia V6T 1Z4, Canada*
[11]*Max Planck Institute for Chemical Physics of Solids, Nöthnitzer Straße 40, 01187 Dresden, Germany*
[12]*Stanford Synchrotron Radiation Lightsource, SLAC National Accelerator Laboratory, Menlo Park, California 94025, USA*
[13]*Materials Science and Technology Division, Oak Ridge National Laboratory, Oak Ridge, Tennessee 37831, USA*
[14]*Department of Electrical and Computer Engineering, Rice University, Houston, Texas 77005, USA*
[15]*Smalley-Curl Institute, Rice University, Houston, Texas 77005, USA*
[16]*Department of Materials Science and NanoEngineering, Rice University, Houston, Texas 77005, USA*
[17]*Department of Chemistry, University of Missouri, Columbia, Missouri 65211, USA*

In the iron-based superconductors, unconventional superconductivity emerges in proximity to intertwined electronic orders consisting of an electronic nematic order and a spin density wave (SDW). Recently, $BaNi_2As_2$, like its well-known iron-based analog $BaFe_2As_2$, has been discovered to host a symmetry-breaking structural transition but coupled to a unidirectional charge density wave (CDW) instead of SDW, providing a novel platform to study intertwined orders. Here, through a systematic angle-resolved photoemission spectroscopy study combined with a detwinning $B_{1g}$ uniaxial strain, we identify distinct spectral evidence of band evolution due to the structural transition as well as CDW-induced band folding. In contrast to the nematicity and spin density wave in $BaFe_2As_2$, the structural and CDW order parameters in $BaNi_2As_2$ are observed to be strongly coupled and do not separate in the presence of uniaxial strain. Furthermore, no nematic band splitting is resolved above the structural transition. Our measurements point to a likely lattice origin of the CDW order in $BaNi_2As_2$.

Quantum materials hosting unconventional superconductivity tend to develop complex phase diagrams where multiple electronic orders interact. In the Fe-based superconductors (FeSCs), the ubiquitous intertwined order takes form in a $C_4$-rotational-symmetry-breaking nematic phase and a spin density wave (SDW) [1–3]. The nematic order manifests in a tetragonal to orthorhombic structural transition, identified as electronically driven by a divergent nematic susceptibility from elastoresistance measurements [4]. Additionally, rotational-symmetry breaking is observed in the electronic, magnetic, and optical properties [5–12]. Superconductivity emerges when these competing orders are suppressed by either doping or pressure, resulting in $T_c$ as high as 40 K [13,14].

$BaNi_2As_2$—a nickel-based analog of the well-studied FeSC $BaFe_2As_2$—shares the same high-temperature tetragonal phase [15]. Distinct from $BaFe_2As_2$, $BaNi_2As_2$ is nonmagnetic and superconducts with a $T_c$ of 0.6 K [16]. Instead of the coupled nematicity and SDW found in $BaFe_2As_2$, $BaNi_2As_2$ exhibits a symmetry-lowering structural transition into a triclinic phase at $T_S = 136$ K accompanied by unconventional charge density waves (CDWs). The progression from the tetragonal state to the triclinic state is still under debate. From x-ray diffraction, Lee *et al.* discovered that the CDW first appears in the tetragonal state as an incommensurate order (IC-CDW), then transits to a unidirectional IC-CDW at $T_S$ and then locks into a commensurate order (C-CDW) below $T_S$ [17,18]. The crystal structure in this picture changes from tetragonal directly to triclinic at $T_S$ in a first-order transition. Recent dilatometry work suggests that the crystal structure explicitly breaks $C_4$ rotational symmetry in

*mingyi@rice.edu
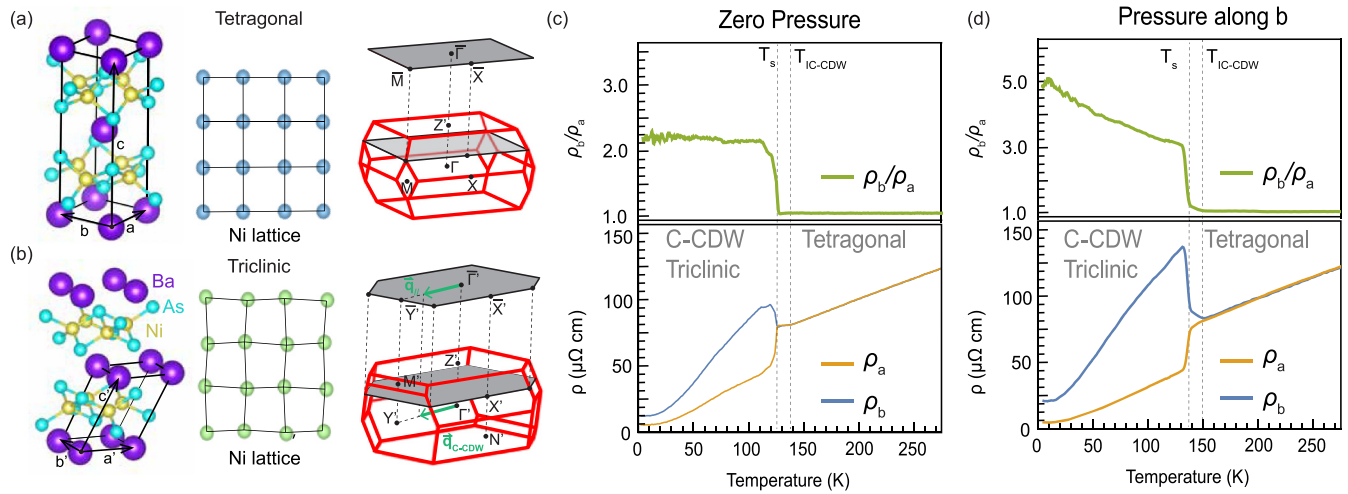
FIG. 1. (a), (b) Crystal structure and BZ for the tetragonal and triclinic phases. The red (gray) BZ represents the 3D (2D projected) BZ. The green arrows in (b) denote the $q$ vectors for C-CDW and its in-plane component. (c), (d) Temperature-dependent in-plane resistivity $\rho_a$ (yellow), $\rho_b$ (blue), and $\rho_b/\rho_a$ (green) with and without uniaxial compressive strain along $b$. Transition temperatures $T_S$ and $T_{\text{IC-CDW}}$ are denoted by the gray dashed lines.

the form of an orthorhombic phase in a second-order transition before additional symmetry lowering into the triclinic phase at $T_S$ in a first-order fashion [19]. Substitution of Co on the Ni site, or Sr on the Ba site, or P on the As site, can completely suppress the triclinic phase and the associated CDW orders, reaching a maximum superconducting $T_c$ of 3.5 K.

Although the hierarchy of the symmetry-breaking orders in $\text{BaNi}_2\text{As}_2$ appears to be similar to $\text{BaFe}_2\text{As}_2$, it is still unclear whether there exists electronically driven nematicity. Elastoresistance measurements show that $\text{Ba}_{1-x}\text{Sr}_x\text{Ni}_2\text{As}_2$ and $\text{BaNi}_2(\text{As}_{1-x}\text{P}_x)_2$ exhibit diverging nematic susceptibilities in the $B_{1g}$ channel. A Ginzburg-Landau analysis suggests that the divergence of nematic susceptibility in $\text{Ba}_{1-x}\text{Sr}_x\text{Ni}_2\text{As}_2$ could be driven by either the lattice or electronic degrees of freedom [20]. In contrast, in $\text{BaFe}_2\text{As}_2$, the divergence in the $B_{2g}$ channel is electronically driven. Reports present conflicting results on which phase transition corresponds to these divergence peaks and whether the associated fluctuations are responsible for the enhancement of $T_c$ at the optimal doping [20,21]. In addition, nematic/IC-CDW fluctuations have been reported for a large temperature window above $T_S$ by studies including Raman scattering [22], inelastic x-ray scattering [23,24], near-edge x-ray absorption fine structure [19], and thermodynamics measurements [25]. Therefore $\text{BaNi}_2\text{As}_2$ and its doping series offer a rich platform to investigate intertwined orders where the electronic structure could provide important insights into the nature of nematicity, CDWs, and their connection to unconventional superconductivity.

Here, using angle-resolved photoemission spectroscopy (ARPES) under uniaxial strain, we reveal the evolution of the electronic structure of $\text{BaNi}_2\text{As}_2$ across its phase transitions. We find evidence of unidirectional band folding consistent with the reported C-CDW wave vector in the C-CDW/triclinic state, and rotational-symmetry breaking that onsets abruptly at the triclinic transition. Furthermore, the extracted temperature evolution of the spectral features identifies a distinct order parameter for the C-CDW from that of the triclinic structural transition. However, the two order parameters are observed to

be strongly coupled even in the presence of uniaxial strain, distinct from the case of $\text{BaFe}_2\text{As}_2$ where strain lifts the onset of the nematic band shift to above that of the SDW order. Our results taken together suggest a strongly lattice-driven intertwined order in parent $\text{BaNi}_2\text{As}_2$ and much weaker nematic fluctuations in a large temperature window compared to that of $\text{BaFe}_2\text{As}_2$.

High-quality single crystals of $\text{BaNi}_2\text{As}_2$ were synthesized using the self-flux method [15]. Resistivity measurements were carried out in a Quantum Design physical properties measurement system using a clamp to supply an in-plane, uniaxial pressure [26]. ARPES measurements were performed at the QMSC beamline at the Canadian Light Source, beamlines 4.0.3, 7.0.2, and 10.0.1 of the Advanced Light Source, and beamline 5-2 of the Stanford Synchrotron Radiation Lightsource with electron analyzers at an energy and angular resolution of 12 meV and 0.1°, respectively. The samples were cleaved *in situ* with base pressures below $5 \times 10^{-11}$ Torr. The polarization used was circular left unless otherwise noted. To avoid the domain-mixing effect, we used a mechanical clamp to detwin the $\text{BaNi}_2\text{As}_2$ crystals along the [010] direction, with a typical pressure of 5–10 MPa [27].

At room temperature, tetragonal $\text{BaNi}_2\text{As}_2$ belongs to the space group $I4/mmm$ ($a = 4.142$ Å, $c = 11.65$ Å) [Fig. 1(a)]. It undergoes a first-order phase transition to the triclinic structure ($a = 4.21$ Å, $b = 3.99$ Å, $c = 6.31$ Å, $\alpha = 105.2°$, $\beta = 108.6°$, $\gamma = 89.3°$, space group $P\bar{1}$) at $T_S = 136$ K [Fig. 1(b)]. The corresponding 3D Brillouin zones (BZs) of the tetragonal and triclinic phases are shown accordingly, where the $C_4$ rotational symmetry is broken for the triclinic phase. The C-CDW $q$ vector in the triclinic state is denoted by $q_{\text{C-CDW}}$, which does not lie in the projected BZ plane, while its in-plane component ($q_{//}$) is very close to one-third of the projected tetragonal BZ (see Supplemental Material [28]). We carried out temperature-dependent in-plane electrical resistivity measurements along the two orthogonal directions with and without uniaxial pressure. In contrast to $\text{BaFe}_2\text{As}_2$ [26], even in the absence of detwinning stress, we observe
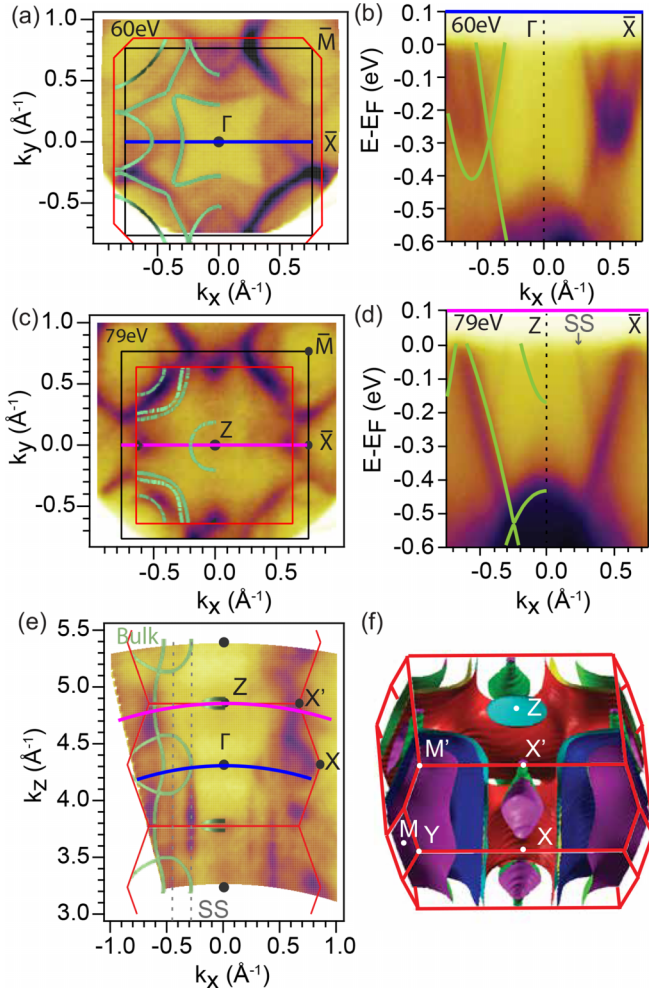
FIG. 2. Electronic structure in the tetragonal state (170 K).
(a) Fermi surface (FS) measured with 60 eV photons ($k_z = 0$).
(b) Band dispersions measured along $\Gamma$-$X$ as marked by the blue lines
in (a) and (e). (c), (d) Same as (a) and (b) but measured with 79 eV
photons ($k_z = \pi$), where band dispersions are measured along $\Gamma$-$Z$ as
marked by the pink lines in (c) and (e). (e) Photon-energy-dependent
measurement in the $k_x$-$k_z$ plane, with an inner potential of 15 eV.
(f) DFT calculation of the 3D FSs. In addition, DFT-calculated band
dispersions and FSs are overlaid on all data in green solid lines. Gray
arrows and dashed lines mark the surface states. All data were taken
with circular-right polarization.



FIG. 3. FSs of detwinned BaNi$_2$As$_2$. (a) FS taken at 79 eV in
the triclinic phase (100 K) with horizontal compressive uniaxial
pressure. (b) Same as (a) but taken in the tetragonal phase (170 K).
(c) Same as (a) but taken at 50 K with a 45° analyzer slit direction.
(d) FS taken with circular-right 60 eV photons at 50 K without uniax-
ial pressure. Blue lines mark the Fermi pockets around $\bar{M}$, while cyan
lines indicate bands folded from the $\bar{M}$ points due to the C-CDW.
(e), (f) MDCs along $k_y = 0.25$ Å$^{-1}$ (solid line) and $k_x = 0.25$ Å$^{-1}$
(dashed line) for the strained sample at 100 K and 170 K respectively,
as marked in (a) and (b). The black arrow denotes the folded feature.

resistivity anisotropy ($\rho_b/\rho_a$) below $T_S$, signaling a strong
structural distortion and associated unequal domain popula-
tions. In the presence of stress, the resistivity anisotropy is
enhanced, demonstrating that the applied uniaxial stress re-
distributes the domain populations. In addition, we observe a
kink above $T_S$ in the zero-stress sample, which corresponds to
the reported IC-CDW or orthorhombic transition [17,21]. In
the measurement under stress, the kink feature is replaced by
the onset of the resistivity anisotropy, which can be interpreted
as either a detwinning effect of the crystal orthorhombic
domains [11] or strain-induced rotational-symmetry break-
ing [29]. It is interesting to point out that, in contrast to
BaFe$_2$As$_2$, the uniaxial pressure does not broaden the struc-
tural transition [26,30]. To visualize the electronic structure
of BaNi$_2$As$_2$, we present ARPES measurements taken in the

tetragonal phase. The Fermi surface maps (FSMs) and band
dispersions along high-symmetry directions corresponding to
the $k_z = 0$ [Figs. 2(a) and 2(b)] and $k_z = \pi$ [Figs. 2(c) and
2(d)] planes are taken with 60 eV and 79 eV photons, re-
spectively [Fig. 2(e)]. The $C_4$ symmetry of the tetragonal
state is observed, with good overall agreement with density
functional theory (DFT) calculations without a renormaliza-
tion factor. The weak correlation effect is consistent with
previous ARPES reports [31,32]. The most intense Fermi
surfaces are large pockets around the $M$ points. As Ni has
two more electrons than Fe, BaNi$_2$As$_2$ is effectively a heavily
electron-doped analog of BaFe$_2$As$_2$ [33]. This can be seen in
the dispersions, where the hole band maxima typically seen
near $E_F$ in BaFe$_2$As$_2$ are approximately 0.5 eV below $E_F$
in BaNi$_2$As$_2$ [Fig. 2(d)]. From a photon energy dependence
study [Fig. 2(e)], we observe $k_z$-dispersive bulk bands, as well
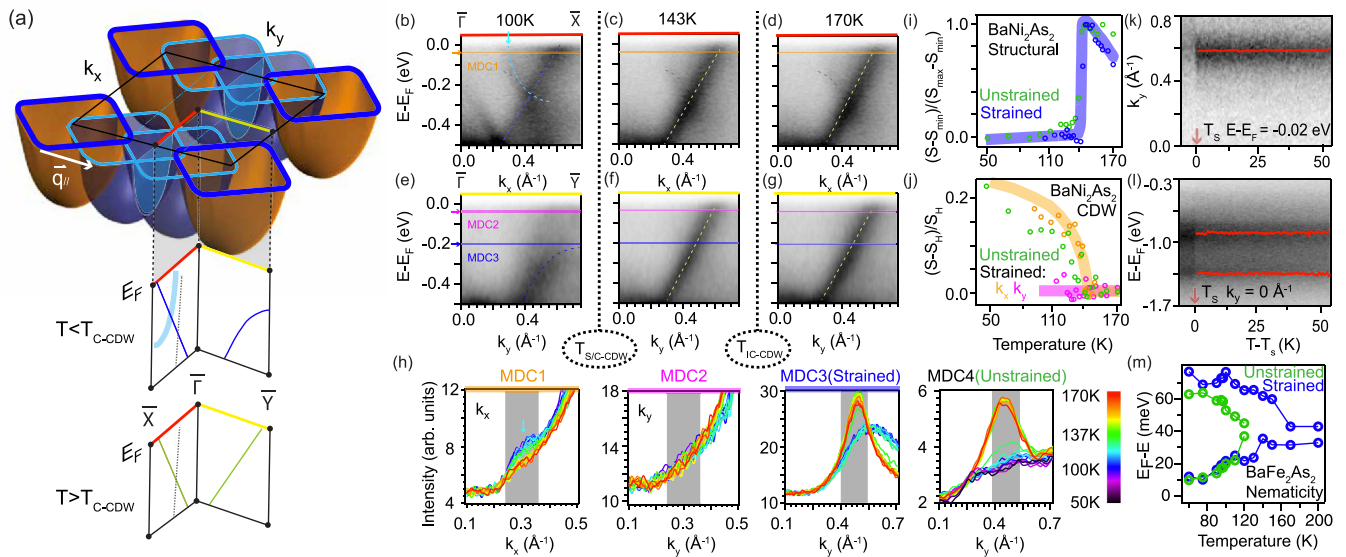
FIG. 4. Temperature evolution through the CDW transitions on detwinned BaNi$_2$As$_2$. (a) Summary of the band evolution across $T_{S/C\text{-}CDW}$. (b)–(d) Temperature dependence of band dispersions along $\bar{\Gamma}$-$\bar{X}$ for (b) $T < T_{S/C\text{-}CDW}$, (c) $T_{S/C\text{-}CDW} < T < T_{IC\text{-}CDW}$, and (d) $T > T_{IC\text{-}CDW}$. (e)–(g) Same as (b)–(d) but taken along $\bar{\Gamma}$-$\bar{Y}$. Dashed lines are guides to the eyes. (h) Temperature dependence of MDCs as marked in (b)–(g). The locations of MDCs are as marked. (i) Integrated spectral weight as a function of temperature within the gray window for MDC3 and MDC4. Each curve is normalized to the maximum spectral weight. (j) Integrated spectral weight within the gray window in MDC1 and MDC2 and the equivalent MDC taken on the unstained crystal as a function of temperature. Each curve is normalized by calculating $(S - S_H)/S_H$, where $S_H$ is the average spectral weight between 145 K and 170 K. Solid lines are guides to the eyes. (k), (l) Continuous temperature evolution of the MDCs and EDCs starting slightly below $T_{S/C\text{-}CDW}$. The red line denotes the peak position by fitting (see Supplemental Material [28]). (m) Temperature evolution of $d_{xz}$ and $d_{yz}$ band positions in BaFe$_2$As$_2$ with and without uniaxial strain (reproduced from [11]).

as nondispersive bands that have no correspondence in the bulk band calculations and must be therefore surface states (denoted by SS).

Having identified the electronic structure in the tetragonal state, we now examine the low-temperature triclinic phase. To probe the intrinsic single-domain electronic structure, we apply uniaxial compressive strain along the crystal axis [010], which aligns all the domains along the shorter $b$ axis. The main features of the low-temperature FSM of the strained crystal [Fig. 3(a)] resemble their tetragonal counterparts except for the appearance of new bands marked in cyan, which can be understood as folded copies of the $M$ pocket that only appear along the $b$ direction, hence breaking the $C_4$ rotational symmetry. This anisotropy can be demonstrated by a comparison of the momentum distribution curve (MDC) taken at equivalent momenta along the $k_x$ and $k_y$ directions, where only a peak is seen across the folded feature [Fig. 3(e)]. Such band folding is a signature of translational-symmetry breaking. We note that the folding vector is approximately $\frac{1}{3}$ of the BZ boundary, which is consistent with the in-plane projection of the $q_{C\text{-}CDW}$ observed by x-ray diffraction [17,31]. Therefore, this band folding is a signature of the unidirectional CDW, which was not observed in previous ARPES studies of BaNi$_2$As$_2$.

To exclude that the rotational-symmetry-breaking effect is due to extrinsic photoemission matrix elements, we measured the strained sample in a geometry where the $a$ and $b$ directions are symmetric with respect to the analyzer slit [Fig. 3(c)]. In this geometry, the photoemission matrix elements are equivalent along the $k_x$ and $k_y$ directions therefore any observed

difference must be intrinsic to the band structure. We note that the folded bands still only appear along the strained direction, reflecting a true $C_2$ symmetry. In addition, above the CDW ordering temperature [Fig. 3(b)], the folded bands in the strained sample disappear, restoring the $C_4$ symmetry, as also confirmed by the disappearance of the peak in the MDC [Fig. 3(e)]. For comparison, the FSM of an unstrained twinned crystal [Fig. 3(d)] shows folded bands in both directions, consistent with the understanding of unidirectional CDW folding under mixed domains. The comparison between the FSMs of the strained and unstrained crystals clearly establishes that uniaxial strain is effective at detwinning the crystal and important for resolving the observed CDW band folding.

Next, we examine in detail the evolution of the rotational and translational symmetry breaking in the electronic structure. Specifically, we traced the dispersions along the $\bar{\Gamma}$-$\bar{X}$ and $\bar{\Gamma}$-$\bar{Y}$ directions measured on detwinned crystals as a function of temperature (Fig. 4). While dispersions along the two orthogonal directions are identical in the tetragonal phase (170 K), bands are strongly modified in the low-temperature phase (100 K), with band crossing $E_F$ only along $\bar{\Gamma}$-$\bar{X}$ but not along $\bar{\Gamma}$-$\bar{Y}$ [Figs. 4(b)–4(g)]. To understand the observed dispersions, we illustrate with a schematic in Fig. 4(a). In the normal state above $T_{IC\text{-}CDW}$, the Fermi surface consists of large pockets around the $\bar{M}$ points. Two types of transitions occur that modify the bands. First, the structural transition from tetragonal to triclinic is reflected in a broken rotational symmetry, where the blue dispersion bends down along $\bar{\Gamma}$-$\bar{Y}$. Second, the unidirectional CDW folds the $M$ pockets along $k_y$,

resulting in a folded parabolic band (cyan) that only appears along $\bar{\Gamma}$-$\bar{X}$.

We then use the spectral signatures of these two distinct symmetry breakings to trace out their order parameters. First, we trace the spectral signature associated with the rotational-symmetry breaking in the form of the band shift along $\bar{\Gamma}$-$\bar{Y}$. As captured by MDC3 in Figs. 4(e)–4(h), an abrupt change occurs at $T_S$ in a strongly first-order fashion. This is also reflected in the apparent jump in the temperature-dependent spectral weight integrated across the gray momentum range [Figs. 4(h), 4(i)]. Second, we trace the band folding by comparing the MDC across the cyan band for $\bar{\Gamma}$-$\bar{X}$ and $\bar{\Gamma}$-$\bar{Y}$ [Fig. 4(h)]. The presence of the folded band is seen in a hump in the MDC along $\bar{\Gamma}$-$\bar{X}$ (MDC1) but not $\bar{\Gamma}$-$\bar{Y}$ (MDC2). The spectral weight of the hump gradually decreases as the temperature is raised, confirmed by the integrated spectral weight in the marked momentum range plotted against temperature, which mimics the behavior of a second-order phase transition [Fig. 4(j)]. This is in contrast to the abrupt jump of the rotational-symmetry breaking in Fig. 4(i), suggesting that the CDW and triclinic structural transition have distinct order parameters.

Comparing the two extracted order parameters, we note that both appear to onset simultaneously in a single phase transition within our experimental uncertainty, although the CDW band folding order parameter evolves much more smoothly than that of the band shift. This contrast is also apparent in the collapsed MDC curves in Fig. 4(h). The abrupt nature of the onset suggests that the two order parameters correspond to the first-order structural transition at $T_S$ into the triclinic phase and the C-CDW order, respectively. Since a small kink is also observed above $T_S$ in the resistivity indicating the onset of IC-CDW and potential nematic order, we searched for evidence of nematic band shift above $T_S$ via a measurement of the dispersions along $\bar{\Gamma}$-$\bar{Y}$ under a slow continuous temperature ramp. The EDC (energy distribution curve) and MDC evolutions [Fig. 4(k), 4(l)] show no resolvable shift or band folding. From a fitting of these bands, we obtain an upper bound of any potential nematic band shift to be 10 meV as shown in the Supplemental Material [28], much smaller than that observed for the nematic phase in $BaFe_2As_2$ [Fig. 4(m)], and on the scale of shift accountable by the lattice orthorhombicity in $BaFe_2As_2$ [11]. The lack of band folding in the IC-CDW region suggests that the associated order parameter is much smaller than that of the C-CDW order on the sample surface, consistent with a recent STM report that also did not find evidence of IC-CDW [34].

We then study the effect of uniaxial strain on the order parameters extracted from the spectral signatures. The spectral weights acquired from unstrained crystals by following the same procedures described above are plotted in [Figs. 4(i), 4(j)], showing very similar behavior to those obtained on strained samples. In particular, we observe no elevation in the onset temperature of either order parameter during the warming up. This is again in contrast to $BaFe_2As_2$ [Fig. 4(k)], where the uniaxial strain clearly elevates the onset temperature of the observed orbital anisotropy and separates it from the SDW ordering temperature [35]. The results taken together suggest that the translational-symmetry breaking of the C-CDW and the structural transition into the triclinic

phase are strongly coupled in $BaNi_2As_2$, and that nematic fluctuations are much weaker than that in $BaFe_2As_2$. The C-CDW, from a lack of Fermi surface nesting conditions, is likely dominated by lattice. Recent DFT results show that two distinct structures compete due to complex As bonding patterns and drive distortions of the Ni layers which possibly explain the unconventional CDW behavior of the ground state [36].

In the broader context of FeSCs, the coupling of the nematic and magnetic order varies as well. In $BaFe_2As_2$, the structural transition is second order, followed by a first-order magnetic transition. In the structural homolog $SrFe_2As_2$, the structural and magnetic transitions are strongly first order and occur simultaneously. Uniaxial strain also does little in harvesting the nematic fluctuations above $T_S$ [30]. The case of $BaNi_2As_2$ as we demonstrate here appears to be similar in spirit to that of $SrFe_2As_2$, where very weak rotational-symmetry breaking exists above the strong first-order structural transition. However, with the substitution of P on the As site or Sr on the Ba site in $BaNi_2As_2$, nematic fluctuations appear to grow both in the size of the anisotropic thermal expansion above $T_S$ [19], as well as a diverging nematic susceptibility, which has been proposed to be responsible for the enhancement of $T_c$ [20]. The $BaNi_2As_2$ family, therefore, offers a rich platform analogous to the magnetic FeSCs where intertwined order from the charge-nematic sector interacts with superconductivity.

[1] P. Dai, Antiferromagnetic order and spin dynamics in iron-based superconductors, Rev. Mod. Phys. **87**, 855 (2015).

[2] F. Wang, S. A. Kivelson, and D.-H. Lee, Nematicity and quantum paramagnetism in FeSe, Nat. Phys. **11**, 959 (2015).

[3] Q. Wang, Y. Shen, B. Pan, Y. Hao, M. Ma, F. Zhou, P. Steffens, K. Schmalzl, T. R. Forrest, M. Abdel-Hafiez, X. Chen, D. A. Chareev, A. N. Vasiliev, P. Bourges, Y. Sidis, H. Cao, and J. Zhao, Strong interplay between stripe spin fluctuations, nematicity and superconductivity in FeSe, Nat. Mater. **15**, 159 (2016).

[4] J. H. Chu, H. H. Kuo, J. G. Analytis, and I. R. Fisher, Divergent nematic susceptibility in an iron arsenide superconductor, Science **337**, 710 (2012).

[5] S.-H. Baek, D. V. Efremov, J. M. Ok, J. S. Kim, J. van den Brink, and B. Büchner, Nematicity and in-plane anisotropy of superconductivity in $\beta$ - FeSe detected by $^{77}$Se nuclear magnetic resonance, Phys. Rev. B **93**, 180502(R) (2016).

[6] T.-M. Chuang, M. P. Allan, J. Lee, Y. Xie, N. Ni, S. L. Bud'ko, G. S. Boebinger, P. C. Canfield, and J. C. Davis, Nematic electronic structure in the "Parent" state of the iron-based superconductor Ca(Fe$_{(1-x)}$Co$_{(x)}$)$_2$As$_2$, Science **327**, 181 (2010).

[7] C. Dhital, Z. Yamani, W. Tian, J. Zeretsky, A. S. Sefat, Z. Wang, R. J. Birgeneau, and S. D. Wilson, Effect of Uniaxial Strain on the Structural and Magnetic Phase Transitions in BaFe$_2$As$_2$, Phys. Rev. Lett. **108**, 087001 (2012).

[8] C. C. Homes, T. Wolf, and C. Meingast, Anisotropic optical properties of detwinned BaFe$_2$As$_2$, Phys. Rev. B **102**, 155135 (2020).

[9] J. L. Niedziela, D. Parshall, K. A. Lokshin, A. S. Sefat, A. Alatas, and T. Egami, Phonon softening near the structural transition in BaFe$_2$As$_2$ observed by inelastic x-ray scattering, Phys. Rev. B **84**, 224305 (2011).

[10] M. A. Tanatar, E. C. Blomberg, A. Kreyssig, M. G. Kim, N. Ni, A. Thaler, S. L. Bud'ko, P. C. Canfield, A. I. Goldman, I. I. Mazin, and R. Prozorov, Uniaxial-strain mechanical detwinning of CaFe$_2$As$_2$ and BaFe$_2$As$_2$ crystals: Optical and transport study, Phys. Rev. B **81**, 184508 (2010).

[11] M. Yi, D. Lu, J.-H. Chu, J. G. Analytis, A. P. Sorini, A. F. Kemper, and B. Moritz, Symmetry-breaking orbital anisotropy observed for detwinned Ba(Fe$_{1-x}$Co$_x$)$_2$As$_2$ above the spin density wave transition, Proc. Natl. Acad. Sci. USA **108**, 6878 (2011).

[12] J. Zhao, D. T. Adroja, D.-X. Yao, R. Bewley, S. Li, X. F. Wang, G. Wu, X. H. Chen, J. Hu, and P. Dai, Spin waves and magnetic exchange interactions in CaFe$_2$As$_2$, Nat. Phys. **5**, 555 (2009).

[13] Y. Mizuguchi, Y. Hara, K. Deguchi, S. Tsuda, T. Yamaguchi, K. Takeda, H. Kotegawa, H. Tou, and Y. Takano, Anion height dependence of $T_c$ for the Fe-based superconductor, Supercond. Sci. Technol. **23**, 054013 (2010).

[14] H. Takahashi, K. Igawa, K. Arii, Y. Kamihara, M. Hirano, and H. Hosono, Superconductivity at 43 K in an iron-based layered compound LaO$_{(1-x)}$F$_{(x)}$FeAs, Nature (London) **453**, 376 (2008).

[15] A. S. Sefat, M. A. McGuire, R. Jin, B. C. Sales, D. Mandrus, F. Ronning, E. D. Bauer, and Y. Mozharivskyj, Structure and anisotropic properties of BaFe$_{1-x}$Ni$_x$As$_2$ ($x = 0$, 1, and 2) single crystals, Phys. Rev. B **79**, 094508 (2009).

[16] F. Ronning, N. Kurita, E. D. Bauer, B. L. Scott, T. Park, T. Klimczuk, R. Movshovich, and J. D. Thompson, The first order phase transition and superconductivity in BaNi$_2$As$_2$ single crystals, J. Phys.: Condens. Matter **20**, 342203 (2008).

[17] S. Lee, G. De La Peña, S. X. L. Sun, M. Mitrano, Y. Fang, H. Jang, J. S. Lee, C. Eckberg, D. Campbell, J. Collini, J. Paglione, F. M. F. De Groot, and P. Abbamonte, Unconventional Charge Density Wave Order in the Pnictide Superconductor Ba(Ni$_{1-x}$Co$_x$)$_2$As$_2$, Phys. Rev. Lett. **122**, 147601 (2019).

[18] S. Lee, J. Collini, S. X.-L. Sun, M. Mitrano, X. Guo, C. Eckberg, J. Paglione, E. Fradkin, and P. Abbamonte, Multiple Charge Density Waves and Superconductivity Nucleation at Antiphase Domain Walls in the Nematic Pnictide Ba$_{1-x}$Sr$_x$Ni$_2$As$_2$, Phys. Rev. Lett. **127**, 027602 (2021).

[19] M. Merz, L. Wang, T. Wolf, P. Nagel, C. Meingast, and S. Schuppler, Rotational symmetry breaking at the incommensurate charge-density-wave transition in Ba(Ni, Co)$_2$(As, P)$_2$: Possible nematic phase induced by charge/orbital fluctuations, Phys. Rev. B **104**, 184509 (2021).

[20] C. Eckberg, D. J. Campbell, T. Metz, J. Collini, H. Hodovanets, T. Drye, P. Zavalij, M. H. Christensen, R. M. Fernandes, S. Lee, P. Abbamonte, J. W. Lynn, and J. Paglione, Sixfold enhancement of superconductivity in a tunable electronic nematic system, Nat. Phys. **16**, 346 (2020).

[21] M. Frachet, P. W. Wiecki, T. Lacmann, S. M. Souliou, K. Willa, C. Meingast, M. Merz, A.-A. Haghighirad, M. L. Tacon, and A. E. Böhmer, Elastoresistivity in the incommensurate charge density wave phase of BaNi$_2$(As$_{1-x}$P$_x$)$_2$, npj Quantum Mater. **7**, 115 (2022).

[22] Y. Yao, R. Willa, T. Lacmann, S.-M. Souliou, M. Frachet, K. Willa, M. Merz, F. Weber, C. Meingast, R. Heid, A.-A. Haghighirad, J. Schmalian, and M. L. Tacon, An electronic nematic liquid in BaNi$_2$As$_2$, Nat. Commun. **13**, 4535 (2022).

[23] Y. Song, S. Wu, X. Chen, Y. He, H. Uchiyama, B. Li, S. Cao, J. Guo, G. Cao, and R. Birgeneau, Phonon softening and slowing-down of charge density wave fluctuations in BaNi$_2$As$_2$, Phys. Rev. B **107**, L041113 (2023).

[24] S. M. Souliou, T. Lacmann, R. Heid, C. Meingast, M. Frachet, L. Paolasini, A.-A. Haghighirad, M. Merz, A. Bosak, and M. L. Tacon, Soft-Phonon and Charge-Density-Wave Formation in Nematic BaNi$_2$As$_2$, Phys. Rev. Lett. **129**, 247602 (2022).

[25] C. Meingast, A. Shukla, L. Wang, R. Heid, F. Hardy, M. Frachet, K. Willa, T. Lacmann, M. L. Tacon, M. Merz, A.-A. Haghighirad, and T. Wolf, Charge-density-wave transitions, phase diagram, soft phonon and possible electronic nematicity: A thermodynamic investigation of BaNi$_2$(As,P)$_2$, arXiv:2207.02294.

[26] J. H. Chu, J. G. Analytis, K. D. Greve, P. L. McMahon, Z. Islam, Y. Yamamoto, and I. R. Fisher, In-plane resistivity anisotropy in an underdoped iron arsenide superconductor, Science **329**, 824 (2010).

[27] I. R. Fisher, L. Degiorgi, and Z. X. Shen, In-plane electronic anisotropy of underdoped '122' Fe-arsenide superconductors revealed by measurements of detwinned single crystals, Rep. Prog. Phys. **74**, 124506 (2011).

[28] See Supplemental Material at http://link.aps.org/supplemental/10.1103/PhysRevB.108.L081104 for the illustration of in-plane components of CDW $q$ vectors for the triclinic and tetragonal phases; temperature evolution of the high-symmetry cuts taken on strained and unstrained samples; continuous temperature evolution of band dispersion of the high-symmetry cuts; EDC analysis of CDW gap.

[29] Y. Song, D. Yuan, X. Lu, Z. Xu, E. Bourret-Courchesne, and R. J. Birgeneau, Strain-Induced Spin-Nematic State and Nematic Susceptibility Arising from $2\times2$ Fe Clusters in $KFe_{0.8}Ag_{1.2}Te_2$, Phys. Rev. Lett. **123**, 247205 (2019).

[30] D. W. Tam, W. Wang, L. Zhang, Y. Song, R. Zhang, S. V. Carr, H. C. Walker, T. G. Perring, D. T. Adroja, and P. Dai, Weaker nematic phase connected to the first order antiferromagnetic phase transition in $SrFe_2As_2$ compared to $BaFe_2As_2$, Phys. Rev. B **99**, 134519 (2019).

[31] N. S. Pavlov, T. K. Kim, A. Yaresko, K.-Y. Choi, I. A. Nekrasov, and D. V. Evtushinsky, Weakness of correlation effect manifestation in $BaNi_2As_2$: An ARPES and LDA + DMFT study, J. Phys. Chem. C **125**, 28075 (2021).

[32] B. Zhou, M. Xu, Y. Zhang, G. Xu, C. He, L. X. Yang, F. Chen, B. P. Xie, X.-Y. Cui, M. Arita, K. Shimada, H. Namatame, M. Taniguchi, X. Dai, and D. L. Feng, Electronic structure of $BaNi_2As_2$, Phys. Rev. B **83**, 035110 (2011).

[33] J. Huang, Z. Wang, H. Pang, H. Wu, H. Cao, S.-K. Mo, A. Rustagi, A. F. Kemper, M. Wang, M. Yi, and R. J. Birgeneau, Flat-band-induced itinerant ferromagnetism in $RbCo_2Se_2$, Phys. Rev. B **103**, 165105 (2021).

[34] T. Qin, R. Zhong, W. Cao, S. Shen, C. Wen, Y. Qi, and S. Yan, Real-space observation of unidirectional charge density wave and complex structural modulation in the pnictide superconductor $Ba_{1-x}Sr_xNi_2As_2$, Nano Lett. **23**, 2958 (2023).

[35] Y. Song, S. V. Carr, X. Lu, C. Zhang, Z. C. Sims, N. F. Luttrell, S. Chi, Y. Zhao, J. W. Lynn, and P. Dai, Uniaxial pressure effect on structural and magnetic phase transitions in NaFeAs and its comparison with as-grown and annealed $BaFe_2As_2$, Phys. Rev. B **87**, 184511 (2013).

[36] B.-H. Lei, Y. Guo, Y. Xie, P. Dai, M. Yi, and D. J. Singh, Complex structure due to as bonding and interplay with electronic structure in superconducting $BaNi_2As_2$, Phys. Rev. B **105**, 144505 (2022).